Physical Properties of Human Polynucleotide Kinase: Hydrodynamic and Spectroscopic Studies †

ARTICLE *in* BIOCHEMISTRY · NOVEMBER 2001

Impact Factor: 3.02 · DOI: 10.1021/bi011383w · Source: PubMed

4 AUTHORS, INCLUDING:

Feridoun Karimi-Busheri
Erciyes Üniversitesi and university of alberta
40 PUBLICATIONS **2,039** CITATIONS
SEE PROFILE

Carol E Cass
University of Alberta
303 PUBLICATIONS **11,420** CITATIONS
SEE PROFILE

Michael Weinfeld
University of Alberta
146 PUBLICATIONS **6,230** CITATIONS
SEE PROFILE

Physical Properties of Human Polynucleotide Kinase: Hydrodynamic and Spectroscopic Studies†

Rajam S. Mani,*,‡,§ Feridoun Karimi-Busheri,‡,§ Carol E. Cass,‡,§,|| and Michael Weinfeld*,‡,§

Experimental Oncology, Cross Cancer Institute, and Departments of Oncology and Biochemistry, University of Alberta, Edmonton, Alberta T6G 1Z2, Canada

Received July 2, 2001; Revised Manuscript Received August 27, 2001

ABSTRACT: Human polynucleotide kinase (hPNK) is a putative DNA repair enzyme in the base excision repair pathway required for processing and rejoining strand-break termini. This study represents the first systematic examination of the physical properties of this enzyme. The protein was produced in *Escherichia coli* as a His-tagged protein, and the purified recombinant protein exhibited both the kinase and the phosphatase activities. The predicted relative molecular mass (M_r) of the 521 amino acid polypeptide encoded by the sequenced cDNA for PNK and the additional 21 amino acids of the His tag is 59 538. The M_r determined by low-speed sedimentation equilibrium under nondenaturing conditions was 59 600 ± 1000, indicating that the protein exists as a monomer, in contrast to T4 phage PNK, which exists as a homotetramer. The size and shape of hPNK in solution were determined by analytical ultracentrifugation studies. The protein was found to have an intrinsic sedimentation coefficient, $s^0_{20,w}$, of 3.54 S and a Stokes radius, R_s, of 37.5 Å. These hydrodynamic data, together with the M_r of 59 600, suggest that hPNK is a moderately asymmetric protein with an axial ratio of 5.51. Analysis of the secondary structure of hPNK on the basis of circular dichroism spectra, which revealed the presence of two negative dichroic bands located at 218 and 209 nm, with ellipticity values of −7200 ± 300 and −7800 ± 300 deg·cm^2·dmol^{-1}, respectively, indicated the presence of approximately 50% β-structure and 25% α-helix. Binding of ATP to the protein induced an increase in β-structure and perturbed tryptophan, tyrosine, and phenylalanine signals observed by aromatic CD and UV difference spectroscopy.

Mammalian polynucleotide kinase (PNK)[1] has the capacity to phosphorylate DNA at 5′-OH termini by catalyzing the transfer of the γ-phosphate of ATP to DNA. The enzyme can also act as a DNA 3′-phosphatase. Since PNK was first purified, it was reasoned that one of its functions would be in DNA repair. Both 3′-phosphate and 5′-OH termini can be generated by ionizing radiation (*1*, *2*) and would require modification to allow DNA polymerases and DNA ligases to seal the strand. Similarly, inhibitors of topoisomerase I, such as camptothecin, can generate strand breaks with 5′-OH groups and possibly, after the removal of the blocked topoisomerase I, 3′-phosphate groups (*3*). Recent evidence indicates that PNK can interact with several members of the base excision repair pathway, namely, XRCC1, DNA polymerase β, and DNA ligase III (*4*).

Mammalian DNA kinases have been purified from a variety of sources including rat liver and testes and calf thymus (*5*−*16*). The isolated enzymes exhibit similar characteristics with regard to the kinase activity including an acidic pH (5.5−6.0) optimum and the minimum size of oligonucleotide that can be phosphorylated, which is 8−12 nucleotides (*8*−*12*). However, there is discrepancy in the reported relative molecular mass (M_r) of these enzymes. Several reports suggested that PNK purified from rat organs exists as a homodimer with an M_r of 80 000 composed of 40 000 M_r polypeptides (*6*, *7*), but PNK activity in tissue extracts detected on activity gels suggested an M_r of 60 000 for the polypeptide (*17*). Values of 56 000−70 000 have been reported for calf thymus PNK (*13*, *14*), while the cDNA for the human protein encodes a protein predicted to have an M_r of 57 100 (*18*, *19*).

Related phosphatases and kinases have also been isolated from other organisms including *Saccharomyces cerevisiae* (*20*), maize (*21*), and phage T4 infected bacteria (*22*, *23*). There is only limited sequence similarity between these proteins. In the case of the T4 enzyme, sequence similarity to the human protein is restricted to short domains associated with ATP binding and phosphatase activities (*18*, *19*). The biochemical and biophysical properties of phage T4 PNK have been well characterized (*24*). Like the mammalian PNK, it has both 5′-kinase and 3′-phosphatase activities. T4 PNK has a broader substrate selectivity, being able to phosphorylate RNA, DNA, and 3′-mononucleotides, but unlike the mammalian protein, it shows a marked preference for sterically exposed 5′-OH groups, such as 5′-overhanging termini (*8*). The phage PNK exists as a homotetramer (M_r = 147 000) with a subunit relative molecular mass of 33 200, and the protein is functionally active in its tetrameric

† This work was supported by a grant (MT-15385) from the Canadian Institutes of Health Research.

* To whom correspondence should be addressed.
‡ Experimental Oncology, Cross Cancer Institute.
§ Department of Oncology, University of Alberta.
|| Department of Biochemistry, University of Alberta.

[1] Abbreviations: BSA, bovine serum albumin; CD, circular dichroism; DTT, dithiothreitol; His tag, histidine tag; PCR, polymerase chain reaction; PNK, polynucleotide kinase; SDS, sodium dodecyl sulfate.

10.1021/bi011383w CCC: $20.00
Published on Web 10/03/2001

state but not in its monomeric state (*24*−*26*). This work represents the first biophysical characterization of a mammalian PNK. We have carried out detailed hydrodynamic studies on human PNK in order to establish its oligomeric state in nondenaturing medium under enzyme assay conditions and have also looked at the effect of ATP binding on the size and shape of the protein. In addition, circular dichroism and UV difference spectroscopy were utilized to examine the effect of ATP binding on protein conformation. Our data indicate that ATP induced conformational changes associated with an increase in β-structure and increased exposure of aromatic amino acids to solvent.

MATERIALS AND METHODS

Purification of Recombinant hPNK from Escherichia coli. The cDNA was amplified by PCR, subcloned in pET-16b (Novagen, Madison, WI), and expressed in *E. coli* as previously described (*19*), except that we used *E. coli* strain BL21-CodonPlus (Stratagene, La Jolla, CA) in place of BLR-(DE3). The bacteria from 4 L were harvested by centrifugation at 5000*g* for 5 min and resuspended in 400 mL of extraction buffer (50 mM Tris-HCl, pH 8.0, and 6 mM 2-mercaptoethanol). Lysozyme was added to a final concentration of 100 μg/mL together with Triton X-100 (final concentration, 0.1%), and after incubation at 37 °C for 15 min, the bacteria were disrupted by sonication. The soluble fraction was separated from the insoluble fraction by centrifugation at 12000*g* for 15 min at 4 °C. Attempts to purify the protein by Ni affinity chromatography resulted in a marked loss of enzymatic activity, and we, therefore, resorted to a more conventional protocol. The soluble fraction was subjected to precipitation by 65% ammonium sulfate followed by centrifugation at 10000*g* for 15 min. The pellet was resuspended in a minimum volume of buffer A [10 mM sodium phosphate, pH 7.3, 0.2 M NaCl, and 4 mM 2-mercaptoethanol, protease inhibitor cocktail (Sigma, St. Louis, MO)] and dialyzed overnight in the same buffer. The solution was loaded on an 80 mL SP-Sepharose Fast Flow cation-exchange column (Amersham Pharmacia BioTech, Baie d'Urfé, PQ). The column was washed with 250 mL of buffer A, and the enzyme was eluted with an 800 mL linear gradient of buffer A containing 0.2−0.8 M NaCl. Fractions containing PNK activity eluted between 0.4 and 0.6 M NaCl. The active fractions were pooled and concentrated by 65% ammonium sulfate. The precipitate was dissolved in buffer A and applied on a HiLoad 16/60 Superdex 75 gel filtration column (Amersham Pharmacia BioTech). The active fractions were pooled and applied on a 5 mL Econo-Pac CHT-II cartridge column (hydroxyapatite) (Bio-Rad, Mississauga, ON). The column was washed with 20 mL of buffer A, followed by running a 60 mL gradient from 0.2 to 0.4 M NaCl. The active fractions appear as a single polypeptide of 60 kDa when analyzed on a 10% SDS−polyacrylamide gel stained with Coomassie Blue or silver staining. The purified protein possessed both 3′-phosphatase and 5′-kinase activities measured as previously described (*19*).

Hydrodynamic Studies. Fringe counts were performed using a Beckman XLI analytical ultracentrifuge and double-sector capillary synthetic boundary sample cells as described (*27*). Prior to ultracentrifugation, protein samples were dialyzed for 48 h in 50 mM Tris-HCl buffer (pH 7.5), 100 mM NaCl, 5 mM $MgCl_2$, and 1 mM DTT. The absorbance of each sample was measured using 1.0 cm path length cuvettes. Samples (150 μL) were loaded into one sector of the sample cell, and 400 μL of the dialysate was loaded into the other sector. Runs were performed at 8000 rpm, and scans were taken when fringes were resolved across the boundary region between protein solution and solvent. The number of fringes produced across the boundary was measured and converted to concentration using an average increment of 3.31 fringes mg^{-1} mL^{-1}. From a plot of the number of fringes versus optical density, a value of 12.2 was established as the extinction coefficient, $\epsilon^{1\%}{}_{1\ cm,280nm}$, for the protein.

Sedimentation Velocity Measurements. Sedimentation velocity experiments were carried out at 20 °C and 50 000 rpm using the XLI analytical ultracentrifuge and interference optic following the procedures described by Laue and Stafford (*28*) and as also outlined in the instruction manual (Spinco Business Center of Beckman Instruments, Inc., Palo Alto, CA). Four hundred microliters of sample solution and 400 μL of dialysate were loaded into two-sector CFE centerpiece sample cells containing sapphire windows. Runs were performed for 4 h, during which a minimum of 30 scans were taken. The sedimentation velocity data were analyzed according to Williams et al. (*29*) to determine the sedimentation coefficient, *s*. The intrinsic sedimentation coefficient, $s^0_{20,w}$, which represents the sedimentation coefficient corrected to water at 20 °C was then calculated from the observed *s* value as described by Laue et al. (*30*).

Sedimentation Equilibrium Studies. Sedimentation equilibrium experiments were carried out at 5 °C using interference optics. Samples (110 μL) were loaded into 6-sector CFE cells, allowing three concentrations of sample to be run simultaneously. Runs were performed at 14 000, 18 000, and 22 000 rpm, and each speed was maintained until there was no significant difference in scans taken 2 h apart to ensure equilibrium was achieved. The sedimentation equilibrium data were evaluated with the Nonlin analysis program using a nonlinear least-squares curve-fitting algorithm (*31*). The program Sednterp (Sedimentation Interpretation Program, version 1.01) was employed to calculate the partial specific volume of the protein from the amino acid composition using the method of Cohn and Edsall (*32*).

Hydrodynamic Calculations and Ellipsoid Modeling. The observed sedimentation coefficient, *s*, determined from sedimentation velocity data will correspond to the maximum *s* value that can be obtained for the given molecular mass of the protein, and correspondingly the protein would have the minimum frictional coefficient, f_0. Translational frictional ratios (f/f_0) were calculated from the experimental Stokes radius obtained from sedimentation velocity experiments ($R_{s,sed}$) according to Mani and Kay (*33*). The frictional ratio f/f_0, which is equivalent to $s_{max}/s_{20,w}$, indicates the maximum shape asymmetry of the protein. The total shape asymmetry depends on two factors, a geometrical shape asymmetry and expansion due to hydration. From f/f_0 or f/f_{shape} values, one can model a globular protein with different ellipsoid shapes (*30*), using the software program Sednterp 1.01, in which the semimajor to semiminor (a/b) axial ratio of a prolate or oblate ellipsoid of revolution is determined using respective power series approximation of the tabulated data for a/b as a function of ($f/f_0 - 1$) or ($f/f_{shape} - 1$) for each ellipsoid. However, one has to designate a δ value, which corresponds to hydration in grams of water per gram of protein, on the

basis of the amino acid composition of the protein for Sednterp to calculate f/f_{shape}. This program provides a graphical presentation of the hydrodynamic model from the volume of an ellipsoid ($^4/_3\pi ab^2$) which is equivalent to the volume of the hydrated protein.

UV Spectroscopy. UV absorption and UV difference spectra were recorded on a Perkin-Elmer Lambda 5 spectrophotometer over the wavelength range 320−250 nm with 1 cm path length cells as described previously (*34*). To generate a UV difference spectrum, both the sample cell and the reference cell contained ATP (10 μM) and hPNK (0.5 mg/mL), but only the contents in the sample cell were mixed, thereby allowing the interaction between PNK and ATP to proceed. Corrections were made for dilutions before the spectrum was analyzed.

Circular Dichroism Spectroscopy. Circular dichroism (CD) measurements were performed in a JASCO J-720 spectropolarimeter (Jasco, Easton, MD) calibrated with a 0.06% solution of ammonium *d*-camphor-10-sulfonate. The temperature in the sample chamber was maintained using a Lauda RM6 low-temperature circulator. Each sample was scanned 10 times, noise reduction was applied, and baseline buffer spectra were subtracted from sample spectra before molar ellipticities were calculated. To obtain spectra in the far-UV region, the cell path length was 0.02 cm and the protein concentration was 0.5 mg/mL, and to obtain the aromatic CD spectra, the cell path length was 1 cm and the protein concentration was 1 mg/mL. The CD spectra were analyzed for secondary structure elements by the Contin ridge regression analysis program of Provencher and Glöckner (*35*). For urea denaturation studies, the changes in the ellipticity values of the protein sample as a function of urea concentration were monitored at 218 nm.

RESULTS

Protein Expression and Purification. Active recombinant hPNK was produced in *E. coli* and purified by sequential chromatography on cation-exchange, gel filtration, and hydroxyapatite columns. The SDS gel, stained with silver nitrate (Figure 1), indicated purification to near homogeneity. The relative molecular mass (M_r) of ~60 000 is consistent with the predicted value of 59 538, including the His tag. The UV absorption spectrum of the His-tagged hPNK (Figure 2) exhibited an absorption maximum at 280 nm, characteristic of tyrosine residues, and a shoulder around 290 nm, characteristic of tryptophan residues. The 280/260 and 280/290 absorbance ratios were 1.66 and 1.31, respectively. Protein concentrations were determined using an extinction coefficient, $\epsilon^{1\%}_{280nm}$, of 12.2, a value that was established by the refractometric method of Babul and Stellwagen (*27*). The His-tagged protein displayed comparable DNA kinase and phosphatase activities to the nontagged protein (data not shown).

Sedimentation Velocity and Sedimentation Equilibrium Studies. In the analytical ultracentrifuge hPNK sedimented as a single symmetrical peak with an $s^0_{20,w}$ value of 3.54 S, which was close to the $s^0_{20,w}$ value of 4.3 predicted for a spherical protein with an M_r 60 000, suggesting that hPNK exists as a monomer. The intrinsic sedimentation coefficient $s^0_{20,w}$ obtained for hPNK in the presence of 10 μM ATP was 3.58, indicating that the protein was not undergoing any

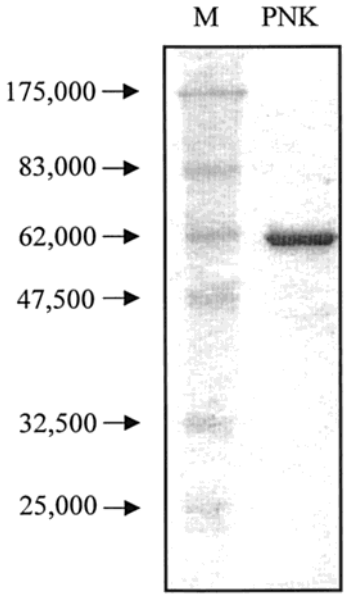

FIGURE 1: SDS gel of purified His-tagged human PNK. The lane marked M shows the size markers.

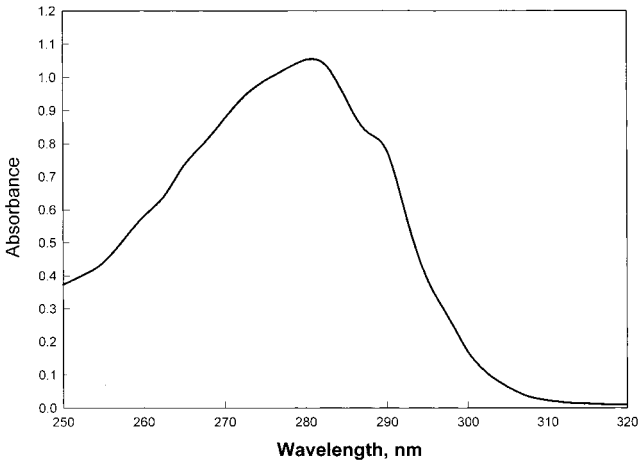

FIGURE 2: UV absorption spectrum of hPNK in 50 mM Tris, pH 7.5, 100 mM NaCl, 5 mM $MgCl_2$, and 1 mM DTT.

aggregation upon ATP binding. The effect of protein concentration on $s_{20,w}$ was studied to ascertain if the protein had a tendency to aggregate at higher concentration. The observed *s* value decreased as the protein concentration increased, as expected for a nonassociating system in which the frictional coefficient increases with an increase in protein concentration. For less asymmetrical proteins, the effect of protein concentration on $s_{20,w}$ can be described using the relationship:

$$s^0_{20,w} = s_{20,w}/(1 - k_s c_p) \quad (1)$$

where the protein concentration (c_p) is in milligrams per milliliter and k_s is an empirical coefficient equal to 0.009 mL/mg for spherical proteins (*36*, *37*). For hPNK, the k_s value was 0.045, suggesting moderate asymmetry. The asymmetry of hPNK was also reflected in its Stokes radius, calculated from sedimentation velocity and sedimentation equilibrium studies. His-tagged hPNK has a Stokes radius of 37.5 Å, whereas bovine serum albumin (BSA), with a M_r of 66 000, possesses a Stokes radius of 35.5 Å (*38*). This result suggests that even though the two proteins do not differ very much

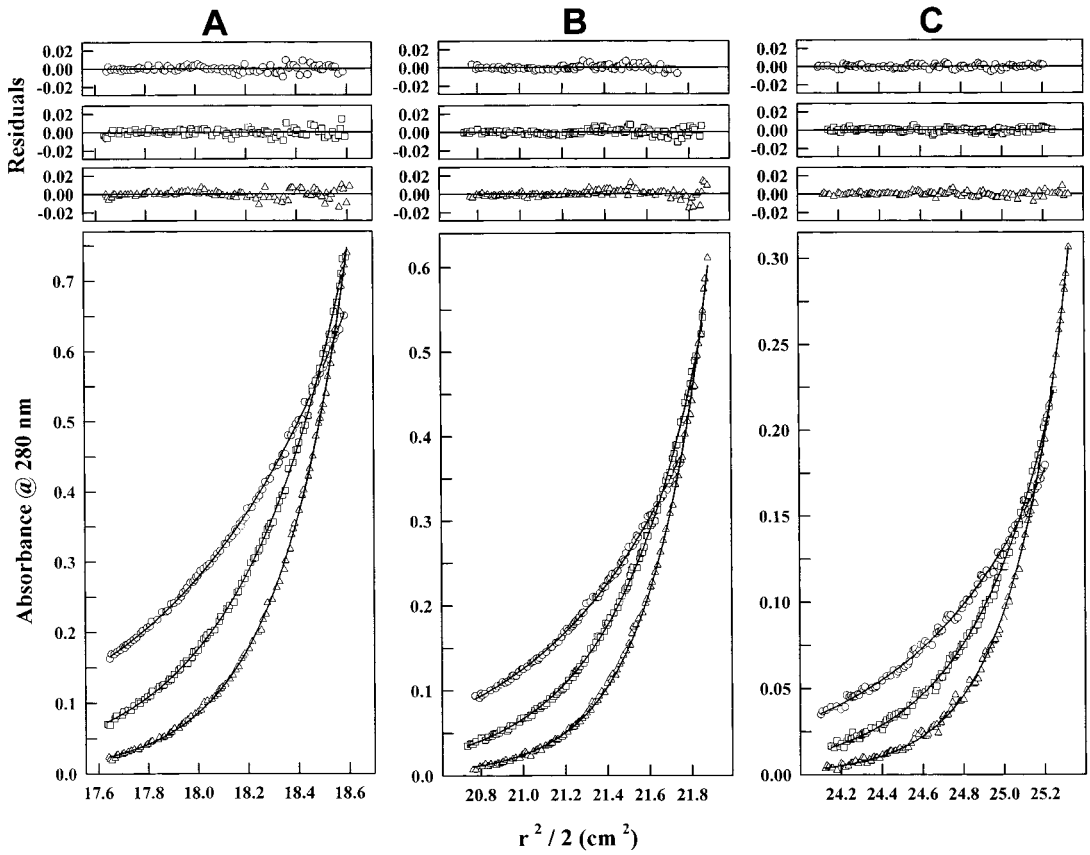

FIGURE 3: Sedimentation equilibrium profiles for hPNK obtained at 14 000 (circles), 18 000 (squares), and 22 000 rpm (triangles) at 5 °C. The samples were run in 50 mM Tris, pH 7.5, 100 mM NaCl, 5 mM $MgCl_2$, and 1 mM DTT for 48 h. The absorbance as a function of radial position for hPNK is shown for the following initial loading concentrations: 0.10 mg/mL (A), 0.2 mg/mL (B), and 0.35 mg/mL (C). Global nonlinear regression fitting of all nine data sets was performed for a single component system, and the solid lines denote the fitted curves. The residuals for each fit are shown in the upper panels above the absorbance vs radial distribution profiles.

in molecular weight, PNK has a more extended conformation and as a consequence sediments more slowly ($s^0_{20,w} = 3.54$) than the globular and more compact BSA ($s^0_{20,w} = 4.6$).

Figure 3 shows the sedimentation equilibrium results and nonlinear regression fits obtained at three different speeds, 14 000, 18 000, and 22 000 rpm, for three initial loading concentrations of 0.1 mg/mL (1.7 μM), 0.2 mg/mL (3.3 μM), and 0.35 mg/mL (6 μM) of PNK. The sedimentation equilibrium data fit well to a single species model with no evidence of any association and a calculated apparent molecular mass of 59 600, implying PNK is monomeric in solution. This agrees very well with the M_r of 60 000 established by SDS gel electrophoresis and the M_r 59 538 predicted for His-tagged hPNK. The M_r in the presence of 20 μM ATP was 60 300 (data not shown), suggesting that hPNK was not undergoing any aggregation upon binding ATP.

Hydrodynamic Properties and Modeling of PNK. On the basis of sedimentation equilibrium and sedimentation velocity studies over a range of concentrations, we can conclude that hPNK exists as a monomer in nondenaturing medium at neutral pH. The combination of the sedimentation coefficient, $s^0_{20,w}$ value, partial specific volume, and molecular weight data allows for a hydrodynamic characterization of hPNK. The Sednterp software program was used to perform the necessary calculations. The results were interpreted in terms of a prolate ellipsoid model, the model used with other DNA binding proteins (*39*). For hydrodynamic modeling one needs to designate a δ value, the hydration factor for Sednterp, to calculate f/f_{shape}. According to Kumosinski and Pessen (*40*), monomeric proteins with an M_r <100 000 will have hydration values close to 0.28 g of H_2O/g of protein based on the increase in hydrodynamic volume over partial specific volume calculated from small-angle X-ray scattering determinations of hydrated volumes of a set of globular proteins. Table 1 provides a summary of the hydrodynamic properties of hPNK and the dimensions of the molecule based on a hydrated prolate ellipsoid model. Figure 4 presents a graphical presentation of this model with the water of hydration as a separate layer along with the model for BSA for comparison (Sednterp program). According to this prolate ellipsoidal model, PNK is moderately asymmetric with an axial ratio of 5.5 (major axis/minor axis), whereas BSA, a globular protein, has an axial ratio of 2.6. Proteins that are asymmetric in nature will sediment more slowly than compact globular proteins due to the increased frictional

Table 1: Hydrodynamic Characterization and Prolate Ellipsoid Modeling of hPNK[a]

$s^0_{20,w}$	3.54 S
sedimentation equilibrium M_r	59600 ± 1000
$R_{s,sed}$	37.5 ± 0.5°A
f/f_0	1.44
f/f_{shape}	1.30
major to minor axis ratio (a/b)	5.51
major axis 2a	18.47 nm
minor axis 2b	3.35 nm

[a] See Materials and Methods section for the computational details used for the hydrodynamic modeling.

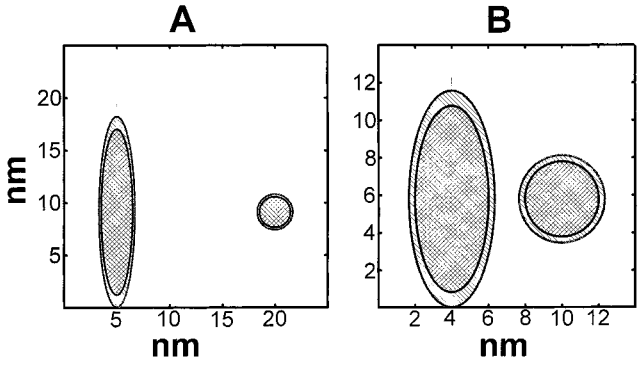

FIGURE 4: Hydrated prolate ellipsoid models for hPNK (A) and BSA (B). This figure shows the size and shape (in nanometers) of the protein and the surrounding layer of hydration. Both a side view (left) and a view down the central axis (right), with the water of hydration displayed as a separate layer on the outside, are represented. Hydration expands the shape of the prolate by 15.69%.

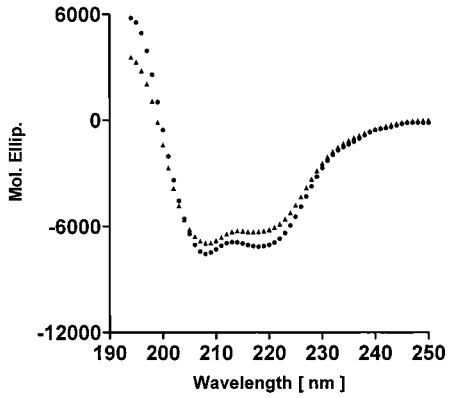

FIGURE 5: Far-UV CD spectrum of hPNK in 50 mM Tris, pH 7.5, 100 mM NaCl, 5 mM $MgCl_2$, and 1 mM DTT (●) and in 50 mM Tris, pH 7.5, 100 mM NaCl, 5 mM $MgCl_2$, 1 mM DTT, and 20 μM ATP (▲).

coefficient. Our sedimentation velocity results were consistent with the hydrodynamic model for these two proteins. PNK had an intrinsic sedimentation coefficient, $s^0_{20,w}$, of 3.54, compared to a value of 4.6 for BSA (*41*), even though their relative molecular masses are in the 60 000 range.

Circular Dichroism Studies. Information concerning the secondary structure of hPNK was obtained from CD data. A typical far-UV CD spectrum of PNK in 0.05 M Tris, pH 7.5, 100 mM NaCl, 5 mM $MgCl_2$, and 1 mM DTT is shown in Figure 5. The protein exhibited two large negative CD bands centered at 218 and 209 nm, and the molar ellipticities, [θ], at these two wavelengths were -7200 ± 300 and -7800 ± 300 deg·cm^2·dmol^{-1}, respectively. The presence of a negative dichroic band at 218 nm indicated the presence of β-structure, in addition to α-helical organization in the enzyme. The CD spectra were analyzed for secondary structural elements by the Contin ridge regression analysis program (*35*). The protein had ~25% α-helix and ~50% β-sheet−β-turn, and the remaining ~25% represented random structure.

Addition of ATP induced a conformational change in hPNK (Figure 5). In the absence of ATP, the molar ellipticity values [θ] at 218 and 209 nm were -7200 ± 300 and -7800 ± 300 deg·cm^2·dmol^{-1}, respectively, and the addition of ATP decreased the ellipticity values to -6300 ± 300 and -7200 ± 300 deg·cm^2·dmol^{-1}, respectively. Analysis of the CD data indicated a decrease in α-helical content accompanied by an increase in β-structure (Table 2). The concentration of ATP used was 20 μM, and the protein to ATP molar ratio was 0.5:1.0, respectively. Similar results were also obtained when the protein to ATP molar ratio was 1:1, i.e., when the ATP level was 10 μM, the concentration used in aromatic CD measurements. Binding of dATP and β,γ-imidoadenosine 5′-triphosphate (AMP-PNP), a nonhydrolyzable form of ATP, which is an inhibitor of kinases (*24*), also produced similar perturbations to the CD spectra (data not shown).

Table 2: Provencher−Glöckner Secondary Structural Analysis of hPNK in the Absence and Presence of ATP

sample	α-helix (%)	β-sheet (%)	β-turn (%)	random (%)
PNK	25	44	5	26
PNK + ATP[a]	19	45	16	20

[a] The concentration of ATP used was 20 μM, and the protein to ATP molar ratio was 0.5:1.0, respectively.

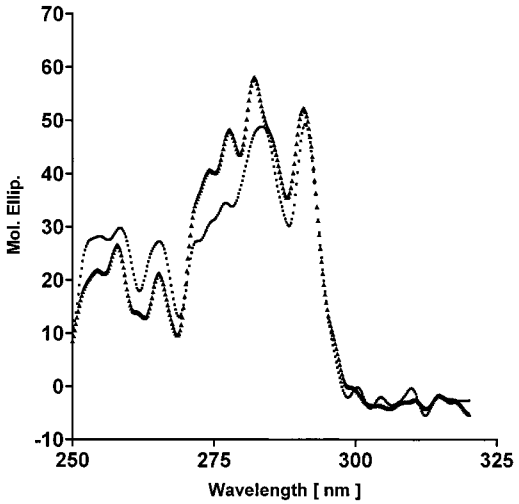

FIGURE 6: Aromatic CD spectra of hPNK in 50 mM Tris, pH 7.5, 100 mM NaCl, 5 mM $MgCl_2$, and 1 mM DTT (■) and in 50 mM Tris, pH 7.5, 100 mM NaCl, 5 mM $MgCl_2$, 1 mM DTT, and 10 μM ATP (▲).

The effect of urea concentration on protein unfolding, in the absence and presence of ATP, was monitored by measuring the ellipticity values at 218 nm. The experiments were performed at room temperature in 50 mM Tris, pH 7.5, 100 mM NaCl, 5 mM $MgCl_2$, and 1 mM DTT. hPNK lost 50% of its starting ellipticity at a urea concentration of 2.5 ± 0.1 M urea, and in the presence of 10 μM ATP, the protein lost 50% of its ellipticity at 2.75 ± 0.1 M urea, suggesting that hPNK is more stable in the presence of ATP. Binding of ATP is also known to protect the enzyme against thermal denaturation and trypsin digestion (*7*).

Near-UV CD Spectra. Near-UV (250−320 nm) CD spectroscopy provides information on the environment of aromatic residues in folded proteins. The aromatic CD spectrum of hPNK in the absence and presence of ATP is shown in Figure 6. The ellipticity of the protein is positive between 260 and 300 nm. The CD band at 291.5 nm is due to tryptophan residues, and the band at 284 nm and a broad shoulder around 279 nm can be assigned to tyrosine residues while the two bands at 268 and 261.5 nm can be attributed to the phenylalanine residues. From the spectrum, it is clear that addition of ATP perturbed the aromatic residues. The

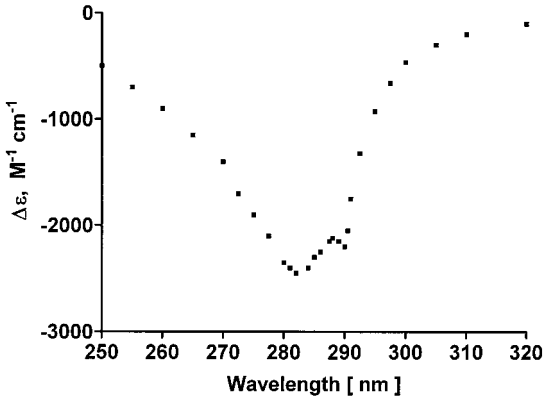

FIGURE 7: UV difference spectrum of hPNK produced by 10 μM ATP. The concentration of hPNK used was 0.5 mg/mL in 50 mM Tris, pH 7.5, 100 mM NaCl, 5 mM $MgCl_2$, and 1 mM DTT. The units are expressed as the difference in molar absorption, $\Delta\epsilon$.

ellipticity value for the CD band at 291.5 nm increased in the presence of ATP. For tyrosine residues, we now observed two, well-resolved CD bands at 284 and 278 nm, as opposed to a broad shoulder around 279 nm for the apoprotein, and the ellipticity values were also higher at these two wavelengths. In the presence of ATP, the CD signals at 268 and 261.5 nm were reduced.

Ultraviolet Difference Spectroscopy. The local environments of aromatic residues in a protein can affect its UV absorption spectrum. If the solvent polarity around an aromatic ring decreases, absorbance maxima will be shifted to longer wavelengths (red shift), and this will result in an increase in molar absorptivity (hyperchromic effect). On the other hand, if the solvent polarity around an aromatic ring increases, absorbance maxima will be shifted to shorter wavelengths (blue shift) and molar absorptivity will decrease (*42*). Hence, UV difference spectroscopy can yield useful information concerning the environment of aromatic residues under varying conditions. The possible effect of ATP on the aromatic amino acids was investigated by measuring UV difference spectra. Figure 7 shows the difference spectrum of hPNK when ATP was added to the sample cell and the contents were mixed, thereby allowing the interaction to proceed, whereas in the reference cell the protein and the buffer containing ATP were not mixed. The concentration of protein and ATP was identical in both cells, except that in the sample cell the protein was able to bind ATP and the observed difference in the absorption spectrum was a consequence of their interaction. The negative difference peak at 290 nm was characteristic of a blue shift of the tryptophan absorption band. The negative trough at 282 nm resulted from a blue shift of the tyrosine absorption band, and these blue shifts associated with tryptophan and tyrosine residues were interpreted as arising from an increased exposure of these aromatic groups to solvent (*43*). The effect of ATP on phenylalanine residues was difficult to detect because the absorption coefficient for phenylalanine is lower than those for tryptophan and tyrosine by an order of magnitude [ϵ ($M^{-1}\cdot cm^{-1}$) for phenylalanine, tryptophan, and tyrosine are 220, 5050, and 1440, respectively]. These findings are in agreement with our near-UV CD data, where we observed changes in the environment of aromatic residues as a consequence of ATP addition. However, with this technique we are also able to monitor the changes in the microenvironment of these aromatic groups as a result of ATP binding.

DISCUSSION

This study provides the first structural characterization of human polynucleotide kinase. We have established by sedimentation under nondenaturing conditions that the protein exists as a monomeric peptide with an M_r of 59 600. Binding of ATP had no significant effect on its sedimentation characteristics, suggesting that the protein was not undergoing any aggregation in the presence of ATP. It is instructive to compare the properties of hPNK to that of T4 phage PNK, the other polynucleotide kinase for which detailed biophysical data have been obtained. Both proteins can phosphorylate 5′-OH termini and dephosphorylate 3′-phosphate termini. However, there is little sequence similarity at the amino acid level, except for short domains associated with ATP binding and phosphatase activity. Unlike hPNK, the phage T4 enzyme can exist in different oligomeric states (*25*, *26*). Sedimentation velocity studies in phosphate and Tris buffers revealed the existence of two sedimenting species with $s_{20,w}$ values of 2.9 and 6.5, indicating the existence of monomeric and tetrameric species. Sedimentation equilibrium studies yielded M_r values of 33 200 and 147 300 for the monomer and the tetramer, respectively. In addition, the T4 enzyme was functionally active only in the tetrameric state while the subunits by themselves had no kinase activity. The secondary structure of hPNK also differs significantly from the phage T4 enzyme. In the case of the T4 enzyme, two negative dichroic bands were positioned at 222 and 209 nm (*25*), and the molar ellipticity values at these two wavelengths were $-20\,000 \pm 1000$ and $-10\,000 \pm 1000$ deg·cm²·dmol^{-1}, respectively, suggesting a highly helical organization of the enzyme. Lillehaug (*25*) estimated the α-helix content to be around 50%, and the amount of β-pleated sheet was approximately 25%, which contrasts with the 25% α-helix and 44% β-pleated sheet determined for hPNK (Table 2).

The substantial structural differences between the two enzymes may explain some of the differences in their respective structure−function relationships. For example, T4 PNK efficiently phosphorylates exposed 5′-OH termini but reacts poorly with recessed 5′-termini in double-stranded substrates. The mammalian enzyme, on the other hand, does not appear to differentiate between exposed and recessed 5′-termini (*8*). This could be rationalized on the basis of a difference in steric hindrance arising from the relative sizes of the two active enzymes.

The CD and UV difference spectroscopy indicated that the binding of ATP to hPNK at micromolar concentration induces a conformational change. In this regard, hPNK is similar to the T4 enzyme, which also binds ATP with high affinity ($k_d = 2\ \mu$M) (*24*). The amino acid sequence of hPNK (*18*, *19*) revealed the presence of a P-loop domain (residues 372−380) commonly associated with ATP binding (*44*). Interestingly, this domain does not contain an aromatic amino acid, although there is a phenylalanine residue at position 381. However, our spectral data (Figures 6 and 7) indicated perturbation of the signals corresponding to tyrosine and tryptophan, as well as phenylalanine, implying that some of these residues come in close proximity to the ATP binding domain. From the observed magnitude of the UV difference

spectrum (molar absorption, $\Delta\epsilon$, at 290 and 282 nm for tryptophan and tyrosine were 2300 and 2500, respectively) (Figure 7), one can quantitate the number of tryptophan and tyrosine residues perturbed by taking into account the molar absorptivity of tryptophan (5050) and tyrosine (1440). We thus estimated that one tryptophan and two tyrosine residues were perturbed and become more exposed to solvent in the presence of ATP. In future studies, fluorescence spectroscopy will be employed to further characterize ATP binding, with a view to establishing its affinity and stoichiometry.

In summary, we have established that the recombinant human polynucleotide kinase, isolated after expressing the PNK cDNA in *E. coli*, exists as a monomer in the buffer system employed for functional activity studies. It thus differs markedly from the tetrameric structure of T4 PNK. Binding of ATP had no significant effect on the sedimentation characteristics of hPNK, suggesting that the protein was not undergoing any aggregation in the presence of ATP. Hydrodynamic modeling indicated the protein to be moderately asymmetric in nature. Spectroscopic analysis showed that hPNK underwent a conformational change upon binding ATP and assumed a more extended structure.

ACKNOWLEDGMENT

We thank Robert Luty for CD analysis, Leslie D. Hicks for performing analytical ultracentrifugation experiments, and Dr. Cyril M. Kay for valuable discussions.

REFERENCES

1. Henner, W. D., Rodriguez, L. O., Hecht, S. M., and Haseltine, W. A. (1983) *J. Biol. Chem. 258*, 711−713.
2. Coquerelle, T., Bopp, A., Kessler, B., and Hagen, U. (1973) *Int. J. Radiat. Biol. Relat. Stud. Phys. Chem. Med. 24*, 397−404.
3. Pouliot, J. J., Yao, K. C., Robertson, C. A., and Nash, H. A. (1999) *Science 286*, 552−555.
4. Whitehouse, C. J., Taylor, R. M., Thistlethwaite, A., Zhang, H., Karimi-Busheri, F., Lasko, D. D., Weinfeld, M., and Caldecott, K. W. (2001) *Cell 104*, 107−117.
5. Pheiffer, B. H., and Zimmerman, S. B. (1982) *Biochem. Biophys. Res. Commun. 109*, 1297−1302.
6. Habraken, Y., and Verly, W. G. (1983) *FEBS Lett. 160*, 46−50.
7. Habraken, Y., and Verly, W. G. (1988) *Eur. J. Biochem. 171*, 59−66.
8. Karimi-Busheri, F., and Weinfeld, M. (1997) *J. Cell. Biochem. 64*, 258−272.
9. Jilani, A., Slack, C., Matheos, D., Zannis-Hadjopoulos, M., and Lasko, D. D. (1999) *J. Cell. Biochem. 73*, 188−203.
10. Ichimura, M., and Tsukada, K. (1971) *J. Biochem. (Tokyo) 69*, 823−828.
11. Teraoka, H., Mizuta, K., Sato, F., Shimoyachi, M., and Tsukada, K. (1975) *Eur. J. Biochem. 58*, 297−302.
12. Levin, C. J., and Zimmerman, S. B. (1976) *J. Biol. Chem. 251*, 1767−1774.
13. Austin, G. E., Sirakoff, D., Roop, B., and Moyer, G. H. (1978) *Biochim. Biophys. Acta 522*, 412−422.
14. Tamura, S., Teraoka, H., and Tsukada, K. (1981) *Eur. J. Biochem. 115*, 449−453.
15. Bosdal, T., and Lillehaug, J. R. (1985) *Biochim. Biophys. Acta 840*, 280−286.
16. Prinos, P., Slack, C., and Lasko, D. D. (1995) *J. Cell. Biochem. 58*, 115−131.
17. Ohmura, Y., Uchida, T., Teraoka, H., and Tsukada, K. (1987) *Eur. J. Biochem. 162*, 15−18.
18. Jilani, A., Ramotar, D., Slack, C., Ong, C., Yang, X. M., Scherer, S. W., and Lasko, D. D. (1999) *J. Biol. Chem. 274*, 24176−24186.
19. Karimi-Busheri, F., Daly, G., Robins, P., Canas, B., Pappin, D. J., Sgouros, J., Miller, G. G., Fakhrai, H., Davis, E. M., Le Beau, M. M., and Weinfeld, M. (1999) *J. Biol. Chem. 274*, 24187−24194.
20. Vance, J. R., and Wilson, T. E. (2001) *J. Biol. Chem. 276*, 15073−15081.
21. Betti, M., Petrucco, S., Bolchi, A., Dieci, G., and Ottonello, S. (2001) *J. Biol. Chem. 276*, 18038−18045.
22. Novogrodsky, A., and Hurwitz, J. (1966) *J. Biol. Chem. 241*, 2923−2932.
23. Midgley, C. A., and Murray, N. E. (1985) *EMBO J. 4*, 2695−2703.
24. Kleppe, K., and Lillehaug, J. R. (1979) *Adv. Enzymol. Relat. Areas Mol. Biol. 48*, 245−275.
25. Lillehaug, J. R. (1977) *Eur. J. Biochem. 73*, 499−506.
26. Wang, L. K., and Shuman, S. (2001) *J. Biol. Chem. 276*, 26868−26874.
27. Babul, J., and Stellwagen, E. (1969) *Anal. Biochem. 28*, 216−221.
28. Laue, T. M., and Stafford, W. F. (1999) *Annu. Rev. Biophys. Biomol. Struct. 28*, 75−100.
29. Williams, J. W., Van Holde, K. E., Baldwin, R. L., and Fujita, H. (1958) *Chem. Rev. 58*, 715−806.
30. Laue, T. M., Shah, B. D., Ridgeway, T. M., and Pelletier, S. L. (1991) in *Analytical Ultracentrifugation in Biochemistry and Polymer Science* (Harding, S. E., Rowe, A. J., and Horton, J. C., Eds.) pp 90−125, Royal Society of Chemistry, Cambridge, U.K.
31. Johnson, M. L., Correia, J. J., Yphantis, D. A., and Halvorson, H. R. (1981) *Biophys. J. 36*, 575−588.
32. Cohn, E. J., and Edsall, J. T. (1943) in *Proteins* (Cohn, E. J., and Edsall, J. T., Eds.) pp 370−381, Reinhold Publishing Corp., New York.
33. Mani, R. S., and Kay, C. M. (1983) *FEBS Lett. 166*, 258−262.
34. Mani, R. S., and Kay, C. M. (1990) *Biochemistry 29*, 1398−1404.
35. Provencher, S. W., and Glöckner, J. (1981) *Biochemistry 20*, 33−37.
36. Creeth, J. M., and Knight, C. G. (1965) *Biochim. Biophys. Acta 102*, 549−558.
37. Kumosinski, T. F., and Pessen, H. (1985) *Methods Enzymol. 117*, 154−182.
38. Siegel, L. M., and Monty, K. J. (1966) *Biochim. Biophys. Acta 112*, 346−362.
39. Ranatunga, W., Lebowitz, J., Axe, B., Pavlik, P., Kar, S. R., and Scovell, W. M. (1999) *Biochim. Biophys. Acta 1432*, 1−12.
40. Kumosinski, T. F., and Pessen, H. (1982) *Arch. Biochem. Biophys. 219*, 89−100.
41. Koenig, V. L., and Pedersen, K. O. (1950) *Arch. Biochem. 25*, 97−108.
42. Donovan, J. W. (1969) in *Physical Principles and Techniques of Protein Chemistry* (Leach, S. J., Ed.) pp 101−170, Academic Press, New York.
43. Donovan, J. W. (1973) *Methods Enzymol. 27*, 497−525.
44. Saraste, M., Sibbald, P. R., and Wittinghofer, A. (1990) *Trends Biochem. Sci. 15*, 430−434.

BI011383W